

## 3D SPH NUMERICAL SIMULATION OF THE WAVE GENERATED BY THE VAJONT ROCKSLIDE

RENATO VACONDIO<sup>(\*)</sup>, SERENA PAGANI<sup>(\*)</sup>, PAOLO MIGNOSA<sup>(\*)</sup> & RINALDO GENEVOIS<sup>(\*\*)</sup>

<sup>(\*)</sup>University of Parma, Department of Civil Engineering - Parco area delle Scienze 181/A, 43121 Parma (Italy)

<sup>(\*\*)</sup>University of Padova, Department of Geosciences - Via Gradenigo 6, 35131 Padova (Italy)

### ABSTRACT

In this paper a 3D numerical modeling of the wave generated by the Vajont slide is presented. In order to completely describe the complex flow generated by the slide a Smoothed Particle Hydrodynamics (SPH) technique was adopted. To the best of the author knowledge this is the first attempt to describe the events adopting a fully 3D numerical model which discretizes the Navier-Stokes Equations.

The SPH adopted herein is a meshless Lagrangian technique which is able to simulate the highly fragmented violent flows generated by the falling slide in the Vajont artificial reservoir. Moreover the Compute Unified Device Architecture (CUDA) of nVidia devices parallelization technique has been adopted to obtain the speed-up sufficient for the high resolution needed to accurately describe the phenomenon.

The simulation results have been validated by comparing the maximum run-up and the water level in the residual lake after the events against the ones reported in literature. In addition to that, the 3D velocity field of the flow during the event together with the discharge hydrograph which overflowed the dam has been obtained.

**KEY WORDS:** *Vajont, rockslide, smoothed particle hydrodynamics, Navier-Stokes, free-surface flows*

### INTRODUCTION

At 22:39 of October 9<sup>th</sup> 1963 a catastrophic rockslide slipped from the northern slope of Mount Toc, on

the border between Friuli Venezia-Giulia and Veneto (Northern Italy), fell into the artificial reservoir of the Vajont dam. The slide generated one of the most destructive waves ever documented in the literature.

The wave overflowed the dam, which remained almost intact, and through the downstream narrow gorge reached the Piave valley and the village of Longarone, causing the loss of about 2000 people.

In the past 50 years the Vajont slide has been deeply analyzed from a geological point of view (SEMENZA *et alii*, 1965; MÜLLER, 1987a; MÜLLER, 1987b; SEMENZA, 2001; GENEVOIS & GHIROTTI, 2005). Several authors investigated also its kinematics and dynamics (HENDRON & PATTON, 1985; SEMENZA & MELIDORO, 1992; ERISMANN & ABELE, 2001) and most of them agree that the rockslide can be schematized as a rigid body (MÜLLER, 1961; SELLI & TREVISAN, 1964; DATEI, 2005; SUPERCHI, 2011). There is also a general agreement (SELLI & TREVISAN, 1964; CIABATTI, 1964; DATEI, 1969) about the total volume of the slide, which was estimated in about  $270\pm 300 \cdot 10^6 \text{ m}^3$ .

On the other hand few studies were devoted to the simulation of the wave generated by the rockslide. The older ones are mainly based on the empirical reconstruction of the wave, through the data collected by eye witnesses and by marks observed on the ground after the disaster (SELLI & TREVISAN, 1964; VIPARELLI & MERLA, 1968; SEMENZA, 2001; DATEI, 2005).

More recently BOSA & PETTI (2010) simulated these phenomenon by means of a 2D Shallow Wa-

ter model. The slide was schematized as a moving vertical wall which acted as a “piston” in moving the water of the Vajont lake. After the halt of the slide the wall was removed from the model and the “before” terrain elevation was substituted with the “after” configuration of the valley.

In the writers’ opinion, however, the wave can be only approximately described by this type of schematization and by means of a two-dimensional depth averaged numerical scheme, which neglects the vertical velocity component and assumes that the pressure is hydrostatic.

On the other hand, three-dimensional Eulerian models, already widespread in other Computational Fluid Dynamic (CFD) fields, are difficult to apply in this case due to the presence of a highly fragmented free surface and due to the computational effort necessary to adequately describe the water body.

In this work a 3D Smoothed Particle Hydrodynamics (SPH) model was used in order to simulate the wave generated by the Vajont rockslide. To the authors’ knowledge, this is the first literature contribution which applies a fully 3D model to the slide movement and to the wave simulation.

The “Smoothed Particle Hydrodynamics” (SPH) is a Lagrangian meshless method originally introduced in astrophysics (GINGOLD & MONAGHAN, 1977) and subsequently extended to Computational Fluid Dynamics (MONAGHAN, 1994).

This numerical technique enables the numerical simulation of free-surface flows with violent impact, such as: breaking waves (DALRYMPLE & ROGERS, 2006), dam-break phenomena (CRESPO *et alii*, 2008), interactions between waves and coastal structures (GÓMEZ-GESTEIRA & DALRYMPLE, 2004), etc.. The main drawback of the SPH technique is the high computational cost which has prevented till now its application to practical engineering problem with complex geometries. Recently CRESPO *et alii* (2011) developed a parallel algorithm named “Dualsphysics” (<http://www.dual.sphysics.org/>) which overcame this limitation by means of the Compute Unified Device Architecture (CUDA) available for nVidia devices. In this way a speed-up of approximately 50-100 with respect of CPU runtime of non-parallel codes was obtained. The same open-source code is herein adopted.

Following the work of SUPERCHI (2011), the 3D shape of the sliding surface and of the rockslide body

were reconstructed. Moreover, assuming that the slide can be described as a rigid body which rotates around an axis, its kinematics has been calculated starting from the Newton’s second law.

The numerical model was validated by comparing the results against: a) the position of maximum wave run-up reported in SEMENZA *et alii* (1965); b) the increased water level of the residual lake after the slide. The discharge hydrograph that overflowed the dam was also evaluated.

## SPH NUMERICAL SCHEME

Through the SPH technique, the continuum is represented as a set of discrete particles, characterized by their own physical properties (such as mass, density, pressure).

The main feature of the SPH technique is to approximate a generic scalar function  $A(\mathbf{r})$  at any point  $\mathbf{r}$ , as follows:

$$A(\mathbf{r}) \cong \int A(\mathbf{r}') W(\mathbf{r}-\mathbf{r}', h) d\mathbf{r}' \quad (1)$$

where  $h$  is the so-called “smoothing length” and  $W(\mathbf{r}-\mathbf{r}', h)$  is the weighting function or kernel. This notation in discrete form becomes:

$$\langle A(\mathbf{r}) \rangle = \sum_b \frac{m_b}{\rho_b} A_b W_{ab} \quad (2)$$

where the summation is extended to all the particles within the domain of influence of the particle  $a$  ( $2h$  for the kernel function herein adopted),  $m_b$  and  $\rho_b$  are respectively the mass and the density of particle  $b$ .

The gradient of the generic scalar function  $A'(\mathbf{r})$  can be approximated by means of an SPH interpolation, as:

$$A'(\mathbf{r}) \cong \int A(\mathbf{r}') W'(\mathbf{r}-\mathbf{r}', h) d\mathbf{r}' \quad (3)$$

which can be written in discrete form as:

$$\langle A'(\mathbf{r}) \rangle \cong \sum_b \frac{m_b}{\rho_b} A_b W'_{ab} \quad (4)$$

In this work the quantic Wendland kernel (WENDLAND, 1995) is adopted:

$$W(\mathbf{r}-\mathbf{r}', h) = \alpha_D \left(1 - \frac{q}{2}\right)^4 (2q+1); \quad 0 \leq q \leq 2 \quad (5)$$

where  $q = \frac{|\mathbf{r}-\mathbf{r}'|}{h}$  and  $\alpha_D$  is  $21/(16\pi h^3)$ .

The movement of the particles is defined by integrating in time the Navier-Stokes equations written for a weakly compressible fluid. In Lagrangian formalism the continuity equation can be written as

$$\frac{D\rho}{Dt} = -\rho \nabla \mathbf{v} \quad (6)$$

where  $\mathbf{v}$  is the velocity vector and  $\rho$  is the density. Discretizing the  $\nabla_{\mathbf{v}}$  by means of the SPH interpolation Equation (6) becomes:

$$\frac{D\rho_a}{Dt} = \sum_b m_b (\mathbf{v}_a - \mathbf{v}_b) \nabla_a W_{ab} \quad (7)$$

where  $\nabla_a W_{ab}$  is the gradient of the kernel function. The summation of Equation (7) is over all the particles within the region of compact support of the kernel function.

The momentum conservation equation in a continuum field is:

$$\frac{D\mathbf{v}}{Dt} = -\frac{1}{\rho} \nabla p + \mathbf{g} + \Theta \quad (8)$$

where  $p$  is the pressure and  $\Theta$  is the dissipative term.

In SPH notation. Equation (8) can be written as:

$$\frac{D\mathbf{v}_a}{Dt} = -\sum_b m_b \left( \frac{p_b}{\rho_b^2} + \frac{p_a}{\rho_a^2} + \pi_{ab} \right) \nabla_a W_{ab} + \mathbf{g} \quad (9)$$

in which  $p_a$  and  $\rho_a$  are respectively the pressure and density for the particle  $a$  (same thing goes for the particle  $b$ ) and  $\pi_{ab}$  is the artificial viscosity (MONAGHAN, 1994) defined as follows:

$$\pi_{ab} = \begin{cases} -\frac{\alpha_v \bar{c}_{ab} \mu_{ab}}{\bar{\rho}_{ab}} & \mathbf{v}_{ab} \cdot \mathbf{r}_{ab} < 0 \\ 0 & \mathbf{v}_{ab} \cdot \mathbf{r}_{ab} \geq 0 \end{cases} \quad (10)$$

with:

$$\mu_{ab} = \frac{h \mathbf{v}_{ab} \cdot \mathbf{r}_{ab}}{\mathbf{r}_{ab}^2 + \eta^2}$$

In Eq. (10)  $\mathbf{r}_{ab} = \mathbf{r}_a - \mathbf{r}_b$ ,  $\mathbf{v}_{ab} = \mathbf{v}_a - \mathbf{v}_b$  being  $\mathbf{r}_k$  and  $\mathbf{v}_k$  the position and the velocity corresponding to particle  $k$  ( $a$  or  $b$ );  $\bar{c}_{ab} = (c_a + c_b)/2$ ,  $\eta^2 = 0.01h^2$ ,  $\alpha_v$  is a free parameter that needs to be tuned. In this work the value of  $\alpha_v = 0.2$  is adopted.

In the SPH method the fluid is simulated as weakly compressible using the following equation of state (BATCHELOR, 1974) which connects pressure  $p$  and density  $\rho$ :

$$p = B \left[ \left( \frac{\rho}{\rho_0} \right)^\gamma - 1 \right] \quad (11)$$

where  $B$  can be written as:

$$B = \frac{(c_0)^2 \rho_0}{\gamma} \quad (12)$$

in which  $\rho_0$  is the reference density (1000 kg/m<sup>3</sup>),  $c_0$  is the speed of sound at the reference density,  $p$  is the pressure and  $\gamma$  is a dimensionless parameter taken equal to 7. In the numerical scheme the speed of sound  $c_0$  is conveniently reduced with respect to its physical value to obtain reasonable time steps (according to the Courant-Friedrichs-Lewy condition). In order to keep

the density variation within the 1%  $c_0$  is set equal to 20 times the maximum expected velocity.

Particle position is updated using the following XSPH velocity correction (MONAGHAN, 1994):

$$\frac{d\mathbf{r}_a}{dt} = \mathbf{v}_a + \varepsilon \sum_b \frac{m_b}{\bar{\rho}_{ab}} \mathbf{v}_{ba} W_{ab} \quad (13)$$

where  $\varepsilon = 0.5$  and  $\bar{\rho}_{ab} = (\rho_a + \rho_b)/2\rho$ . This method moves particle  $a$  with a velocity that is close to the average velocity in its neighborhood.

Time-step  $\Delta t_i$  is calculated according to the Courant-Friedrichs-Lewy condition, the forcing terms and the viscous diffusion terms (MONAGHAN, 1989), so  $\Delta t$  is equal to:

$$\Delta t = CFL \cdot \min(\Delta t_f, \Delta t_{cv});$$

with:

$$\Delta t_f = \min_a \left( \sqrt{h/|f_a|} \right) \quad \Delta t_{cv} = \min_a \frac{h}{c_s + \max_b \left| \frac{h \mathbf{v}_{ab} \cdot \mathbf{r}_{ab}}{\mathbf{r}_{ab}^2} \right|}$$

where  $|f_a|$  is the magnitude of the force per unit of mass for particle  $a$ , and  $\Delta t_{cv}$  combines the Courant and the viscous time-step controls and  $CFL$  is the Courant number. In this work  $CFL = 0.4$  has been used.

Equations (7), (9) and (13) are updated in time using a symplectic time integration algorithm (LEIMKHULER *et alii*, 1996). The values of density and particle position are calculated at the middle of the time step  $n+1/2$  as:

$$\rho_a^{n+1/2} = \rho_a^n + \frac{\Delta t}{2} \frac{d\rho_a^n}{dt},$$

$$\mathbf{v}_a^{n+1/2} = \mathbf{v}_a^n + \frac{\Delta t}{2} \frac{d\mathbf{v}_a^n}{dt},$$

where  $t = n\Delta t$ . Pressure,  $p_a^{n+1/2}$ , is calculated using the equation of state (11). In the second stage the acceleration  $d\mathbf{v}_a^{n+1/2}/dt$  gives the velocity and hence the position at the end of the time step:

$$\mathbf{v}_a^{n+1} = \mathbf{v}_a^{n+1/2} + \frac{\Delta t}{2} \frac{d\mathbf{v}_a^{n+1/2}}{dt}$$

$$\mathbf{r}_a^{n+1} = \mathbf{r}_a^{n+1/2} + \frac{\Delta t}{2} \mathbf{v}_a^{n+1}$$

At the end of the time step  $d\rho_a^{n+1}/dt$  is calculated using the updated values of  $\mathbf{v}_a^{n+1}$  and  $\mathbf{r}_a^{n+1}$ .

The discretization of solid boundary conditions is still an open problem in SPH models. In this work the “dynamic boundary particles” method is adopted (CRESPO *et alii*, 2007). This method guarantees that complex domains can be easily discretized and leads to a good compromise between accuracy and computational costs. The boundaries are discretized by a set

of solid particles that satisfy the same equations of the fluid ones (Equation (7) and (9)), but their position is not calculated using Equation (13) as for the fluid particles. The boundary particles which describe the Vajont valley do not modify their position during the simulation, whereas the boundary particles which discretize the landslide body are moved according to the velocity assigned to the slide.

### KINEMATICS OF THE ROCKSLIDE

Recent and current researches, carried out at the Geosciences Department (University of Padova, Italy), focus on the relationships between the landslide mass before and after the failure event. In particular, the obtained results show that the volume of the slid mass is just a little bit higher than that of the original in-situ mass, the difference being apparently in the range of inevitable errors due to the low accuracy of the pre-failure maps.

Besides, the shape of the sliding surface has been generally assumed as a "chair" shape (SUPERCHI, 2011), but the difference between the real shape and that of the corresponding circular arc has been considered by many Authors negligible.

### GEOMETRY OF THE SLIDE BODY

The 3D geometry of the sliding surface was recently reconstructed by SUPERCHI (2011) and BISTACCHI (2013, present Conference) (see Fig. 1) by analyzing the pre- and post- slide maps and through seismic sections and boreholes stratigraphy interpretation. In the present work the 3D shape of the rockslide body before the fall (Fig. 2) has been defined by intersecting the pre-slide topographical map of SEMENZA *et alii* (1965) with the sliding surface (SUPERCHI, 2011). In such way the volume of the rockslide was estimated of about  $310 \cdot 10^6 \text{ m}^3$ .

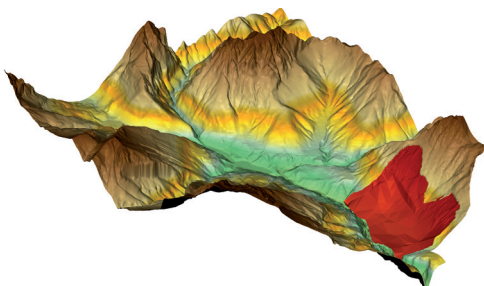


Fig. 1 - Sliding surface 3D view (with the sliding surface in red)

Similarly, the shape of the slide body after the fall has been reconstructed by intersecting the post-slide topography (obtained from Lidar survey data) with the surface obtained by subtracting the volume of the slide from the pre-slide topography (Fig. 1).

Once defined the shape of the rockslide body, the XYZ coordinates of the barycenter in the pre-slide configuration  $\mathbf{b}_{pre}$  has been calculated discretizing the entire volume of the slide by means of  $N$  parallelepiped columns with a regular squared base  $\Delta x = \Delta y = 5 \text{ m}$  and variable height  $d$ . Assuming constant density for the entire mass, the following expression holds:

$$\mathbf{b}_{pre} = \frac{\Delta x^2}{V_{tot}} \sum_{i=1}^N d_i \mathbf{x}_i \quad (14)$$

where  $V_{tot}$  is the total volume of the slide and  $\mathbf{x}_i$  is the vector of coordinates of the center of mass of the  $i$ -th parallelepiped. The coordinates of the barycenter of the rockslide mass after the event,  $\mathbf{b}_{post}$ , was obtained in a similar way. It follows that the distance between the two centers of gravity  $d_b$  is equal to 326 m.

In order to define the movement of the slide from the initial to the final configuration, we made the following assumptions (CIABATTI, 1964; DATEI, 2005):

- the entire mass is concentrated in the barycenter of the slide;
- the barycenter moved from  $\mathbf{b}_{pre}$  to  $\mathbf{b}_{post}$  along a circular arc with radius  $R$  (which needs to be defined);
- the axis of rotation is normal to the vertical plane containing the position of the two centers of gravity.

On the basis of the previous assumptions it follows that the equation in the 3D space of the rotation axis (and so the entire movement of the rockslide, assumed as a rigid body) depends only on the value of the radius  $R$ . In other words, once  $R$  is defined, the coordinate vector of the  $i$ -th point of the mass slide

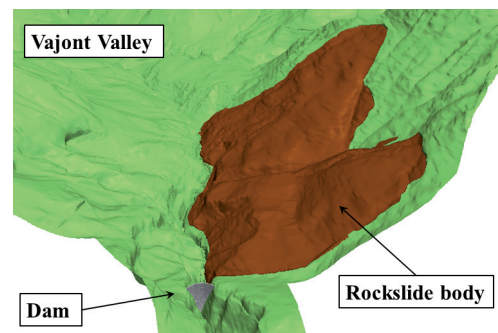


Fig. 2 - Three-dimensional representation of the body rockslide and the valley of the Vajont

at the end of the movement  $\mathbf{x}_i^{rot}$  is defined as follows:

$$\mathbf{x}_i^{rot} = A^{-1}BA(\mathbf{x}_i^{pre} - \mathbf{x}_{cr}) + \mathbf{x}_{cr} \quad (15)$$

where  $\mathbf{x}_i^{pre}$  and  $\mathbf{x}_{cr}$  are, respectively, the coordinate vectors of the  $i$ -th point before the slide and of the intersection point between the vertical plane containing  $\mathbf{b}_{pre}$  and  $\mathbf{b}_{post}$  and the rotation axis of the slide. In (15)  $A$  and  $B$  are defined as:

$$A = \begin{pmatrix} \cos\alpha & \sin\alpha & 0 \\ -\sin\alpha & \cos\alpha & 0 \\ 0 & 0 & 1 \end{pmatrix} \quad (16)$$

$$B = \begin{pmatrix} \cos\gamma & 0 & \sin\gamma \\ 0 & 1 & \sin\gamma \\ -\sin\gamma & 0 & \cos\gamma \end{pmatrix} \quad (17)$$

with:

$$\gamma = 2 \arcsin\left(\frac{d_b}{2R}\right),$$

$$\alpha = \arctan\left(\frac{z_{bpost} - z_{bpre}}{(x_{bpost} - x_{bpre})^2 + (y_{bpost} - y_{bpre})^2}\right).$$

The  $\mathbf{x}_{cr}$  vector can be calculated from the following equation:

$$\mathbf{x}_{cr} = \alpha^{-1} \mathbf{x}' + \mathbf{b}_{pre}$$

with  $\mathbf{x}'$  defined as:

$$x'_{cr} = R \sin\left(\frac{\pi}{2} - \vartheta - \frac{\gamma}{2}\right) \quad (18)$$

$$y'_{cr} = 0$$

$$z'_{cr} = R \cos\left(\frac{\pi}{2} - \vartheta - \frac{\gamma}{2}\right)$$

$$\text{where } \vartheta = \arcsin\left(\frac{d_b}{z_{bpost} - z_{bpre}}\right)$$

Starting from the pre-configuration of the valley and rotating the rockslide mass from the initial to the final position, the virtual post-configuration of the valley is reconstructed. This can be compared against the real topography obtained on the basis of post-slide surveys. The  $L_2$  norm of the differences of the elevations of the two surfaces can be calculated as follows:

$$L_2(R) = \sum_{i=1}^N \sqrt{\frac{(z_i^{rot} - z_i^{post})^2}{N}} \quad (19)$$

where  $z_i^{rot}$  is the elevation of the  $i$ -th point of the virtual surface obtained by rotating the body of the slide from the initial to the final position, and  $z_i^{post}$  the elevation of the same point in the real post-slide topography. The value of the radius  $R$  has been defined by minimizing the norm of Equation (19).

The value of the radius  $R$  which minimizes the

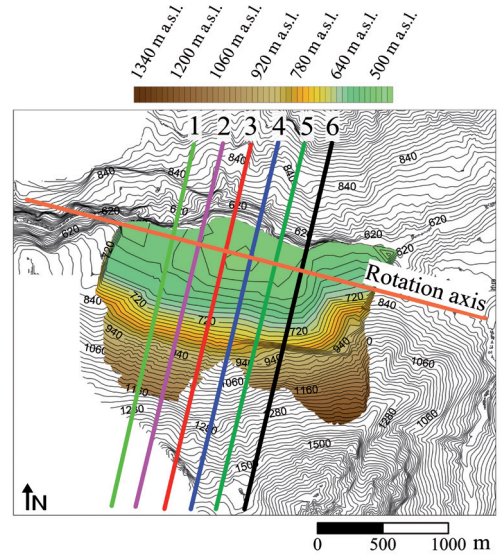


Fig. 3 - Plan traces of some cross-sections shown on the bathymetry of the valley before 1963. The track of the rotational axis is also shown

$L_2(R)$  is equal to 800 m, which correspond to the rotation axis shown in Fig. 3. The value of  $R$  herein obtained substantially agrees with those obtained by DATEI (1969) analyzing different sections of the slide (830 - 912 m).

In Figure 3 the traces of six cross-sections of the Vajont valley are drawn. The cross sections are then plotted in Fig. 4 with the following information:

- the shape of the valley before the slide (SEMENZA *et alii*, 1965 - red line);
- the sliding surface (SUPERCHI, 2011 - blue line);
- the real shape of the valley after the slide (black line);
- the virtual surface of the slide obtained according to the procedure previously described (green line).

From Fig. 4 it can be appreciated that the green line reasonably superimposes with the black one. This means that the assumed rotational movement is able to reproduce the post-slide configuration of the valley starting from the pre-slide configuration. Hence the assumption of considering the rockslide as a rigid object which rotates around an axis is confirmed. The differences between virtual and real topographies are not negligible only in section 1, which is the one closer to the dam. This suggests that in this zone the hypothesis that the landslide is representable as a rigid body is not fully verified.

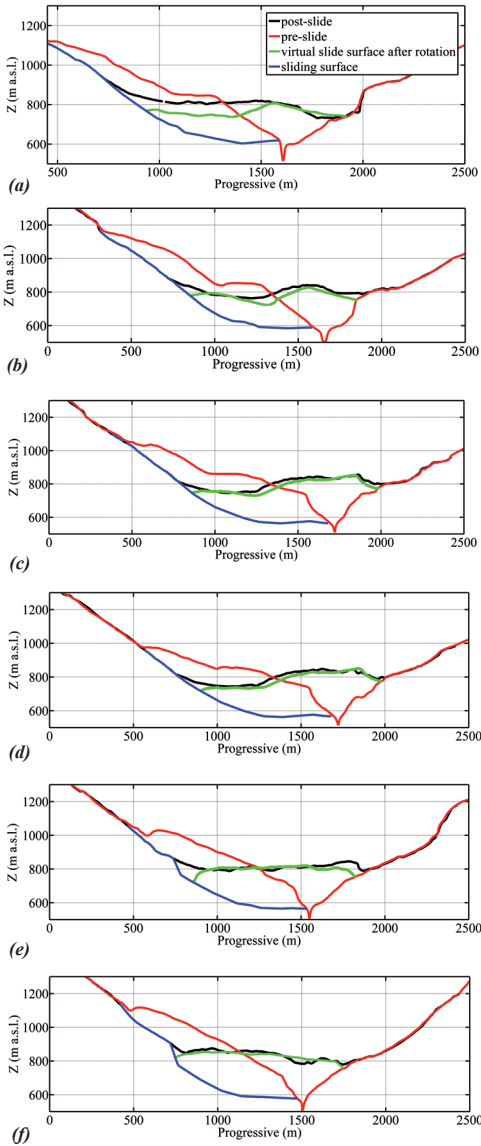


Fig. 4 - Cross-sections (a) n.1, (b) n.2, (c) n.3, (d) n.4, (e) n.5 and (f) n.6

**VELOCITY AND TOTAL TIME OF THE SLIDE**

For the objectives of the present study the most important aspects of the kinematics of the slide are the total duration  $T_p$ , that is the time elapsed between the beginning and end of the movement of the slide and the time history position of the rock mass. By analyzing different 2D slices of the valley and assuming a straight movement of each center of mass CIABATTI (1964) and subsequently SELLI & TREVISAN (1964) es-

$R$ (m)	800
$\alpha_0$ (rad)	0.469
$\alpha_1$ (rad)	0.058
$f$ (-)	0.27
$v_{max}$ (m/s)	18.5
$T_f$ (s)	27.9

Tab 1 - Values of main characteristics of the kinematics of the slide

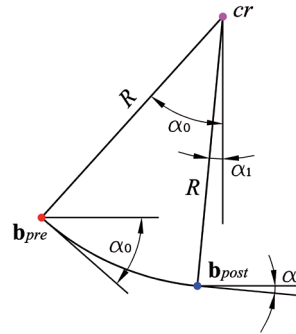


Fig. 5 - Angles  $\alpha_0$  and  $\alpha_1$

timated values of  $T_f$  ranging between 40-45 seconds.

DATEI (1969) performed a critical analysis of the seismogram recorded in Pieve di Cadore (CALOI, 1966) and extended the analysis of SELLI & TREVISAN (1964) assuming that the center of mass of each section moved along a circular arc. Due to this 2D approach, each slice of the slide rotates with a slightly different radius and reaches the final position with different total durations  $T_f$ , all in the range 20-25 seconds. In the present paper the 2D Datei's approach was extended in 3D, obtaining a unique total duration of the slide fall and a unique time history of the rock mass position.

As stated before, we assume that the barycenter of the sliding mass moves in the vertical plane containing  $b_{pre}$  and  $b_{post}$  and along the circular arc with radius  $R$  and center  $x_{cr}$ .

Let's define  $\alpha$  as the generic angle that the tangent to the circular arc passing through the barycenter forms with the horizontal line (the initial and final values  $\alpha_0$  and  $\alpha_1$  are shown in Tab. 1 and Fig. 5).

The velocity magnitude  $|v|$  of the barycenter can then be calculated as follows:

$$|v| = -R \frac{d\alpha}{dt} \tag{20}$$

From the second law of dynamics, it is then possible to derive the following equation of motion for the barycenter:

$$R \frac{d^2\alpha}{dt^2} = -g \left\{ \sin\alpha - f \left( \cos\alpha + \frac{R}{g} \left( \frac{d\alpha}{dt} \right)^2 \right) \right\} \tag{21}$$

where  $f$  is the friction coefficient and  $g$  is the gravity acceleration. We remark that the Equation (21) is obtained assuming that the mass moves from the initial to the final position with a positive velocity ( $da/dt < 0$ ) and also that the force exerted by the water mass on the rockslide body is negligible.

With simple algebraic manipulation on Equation (21), the following differential equation can be obtained (DATEI, 1969):

$$\frac{d^2\alpha}{dt^2} - f \left( \frac{d\alpha}{dt} \right)^2 = -\frac{g}{R} (sen\alpha - fcos\alpha) \tag{22}$$

The term  $-f (da/dt)^2$  is due to the centrifugal force and is from here on neglected because of its small contribution (DATEI, 1969).

Equation (22) can be integrated imposing that that at  $t=0$   $\alpha=\alpha_0$  and at  $t=T_f$   $\alpha=\alpha_1$  and also that  $da/dt=0$  both at  $t=0$  and  $T=f$ . After some algebra (DATEI, 1969) the velocity magnitude  $|v|$  time history can be expressed as:

$$|v| = (\alpha_0 - \alpha_{max}) \sqrt{\frac{gR}{\cos\alpha_{max}}} sen \left( t \sqrt{\frac{g}{R\cos\alpha_{max}}} \right)$$

where  $\alpha_{max}$  is the angle at which the velocity reaches its maximum and it can be calculated as follows:

$$\tan\alpha_{max} = f = -\frac{\cos\alpha_1 - \cos\alpha_0}{\sin\alpha_1 - \sin\alpha_0} \tag{23}$$

The time  $T_f$  at which the barycenter reaches its final position and hence the slide mass stops can be calculated as:

$$T_f = \pi \sqrt{\frac{R\cos\alpha_{max}}{g}} \tag{24}$$

The maximum magnitude of the velocity  $v_{max}$  is obtained as:

$$v_{max} = \sqrt{\frac{2gR}{\cos\alpha_{max}} [1 - \cos(\alpha_0 - \alpha_{max})]} \tag{25}$$

In Table 1 the values of  $f$ ,  $v_{max}$  and  $T_f$  obtained by applying the previous equations are reported.

### NUMERICAL SIMULATIONS AND RESULTS

The initial water elevation in the lake was set at the historical value of the day of the event (about 700 m a.s.l.). The three-dimensional domain (valley slopes, slide and water bodies) was then discretized into cubic cells of side  $\Delta x$  equal to 5 m and with a smoothing length  $h = 1.5 \Delta x$ , leading to the number of particles reported in Table 2.

A preliminary sensitivity analysis of the numerical model has shown that the parameters which remark-

ably influence the main characteristics of the flow are the maximum velocity magnitude of the slide as well as its total duration  $T_f$ .

The values calculated in the previous section ( $T_f = 27.9$  s and  $v_{max} = 18.5$  m/s) were adopted in the very first simulation. However the maximum run-up obtained by the numerical model significantly underestimates the historical one reported by SEMENZA *et alii* (1965). This can be explained by considering that the Equation (22) has been obtained by making significant simplifications of the physical phenomenon. For example the total mass of the slide was concentrated in the barycenter, and thus the effect of the forces exerted on the sliding surface by the valley have been schematized by a time-constant friction coefficient. Moreover the effect of the water body on the rockslide movement was also neglected.

For these reasons, it was decided to simulate different total durations of the slide, modifying the velocity magnitude accordingly.

After some trials, the best results were obtained with a total duration of the slide ( $T_f$ ) equal to 17 seconds, which corresponds to a maximum velocity  $v_{max}$  equal to 30 m/s.

In the following the main results of this simulation were described. Figure 6 shows the plan snapshots of the free surface elevation with a time interval of 10 s, starting from the beginning of the slide movement. After 10 seconds the water already starts to overflow the dam, mainly in the right side of the valley. After 20 seconds the slide movement has already stopped, while the wave front continues to rise the north side of the Vajont valley. The flow begins to divide into four portions: I) one overtops the dam and moves into the Vajont gorge towards the Piave Valley (west), II) the central part continues to climb the right side of the valley (north), III) a small part moves south retracing the valley furrow of Massalazza, and IV) a consistent part propagates toward Erto (east).

At  $t = 30$  seconds the wave reaches the maximum

Type	N. of particles
<i>slopes</i>	2'143'670
<i>slide</i>	127'372
<i>fluid</i>	1'683'364
<i>total</i>	3'954'406

Tab. 2 - Number of particles of the model

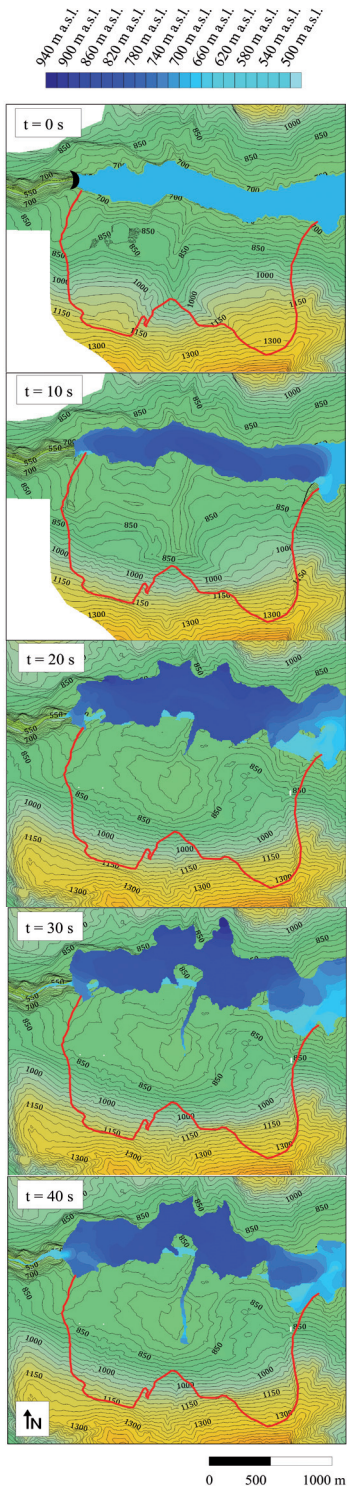


Fig. 6 - Water elevation in the numerical model after 0, 10, 20, 30 and 40 s.

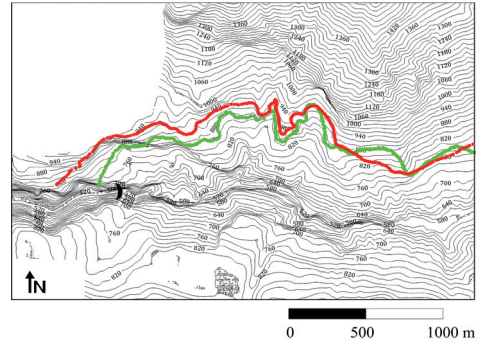


Fig. 7 Experimental (SEMENZA et alii, 1965 - red line) and numerical (green line) run up

run-up on the right side of the valley.

Figure 6 at time 40 s shows the descent of the wave: the flow is partially diverted (by the slide body) to the eastern and western directions. Downstream the dam, the water spreads rapidly in the gorge toward the village of Longarone.

Figure 7 shows the historical (red line - SEMENZA et alii, 1965) and numerical (green line) maximum run-up of the wave. The numerical model is able to reproduce satisfactorily the central and eastern part of the run-up edge. Close and downstream the dam, however, significant differences between historical and numerical results are appreciable. This is probably due to the assumption of the slide as an unique rigid body, which is only approximately true close to the extreme borders (upstream and downstream) of the slide (see also Fig. 4a).

Figure 8 shows six perspective snapshots of the slide and of the wave. In the images the velocity magnitude is mapped by colors. It can be observed that the violent movement of the rockslide creates a complex flow field with a very irregular and fragmented free surface, difficult to be simulated with 3D Eulerian numerical methods, and with 2D SWE codes too.

The maximum speeds on the wave front was estimated of about 35 m/s, while the wave that propagates in the residual lake (towards Erto) reaches a maximum speed of around 20 m/s.

It can be observed that at around 30-40 seconds, when the discharge leaving the dam reaches its maximum, the flow is concentrated in the left hydraulic side of the dam, with maximum water thickness of about 50 m.

This justify the major damages observed on the dam crest on this side.

Due to the high computational cost, it was not possi-



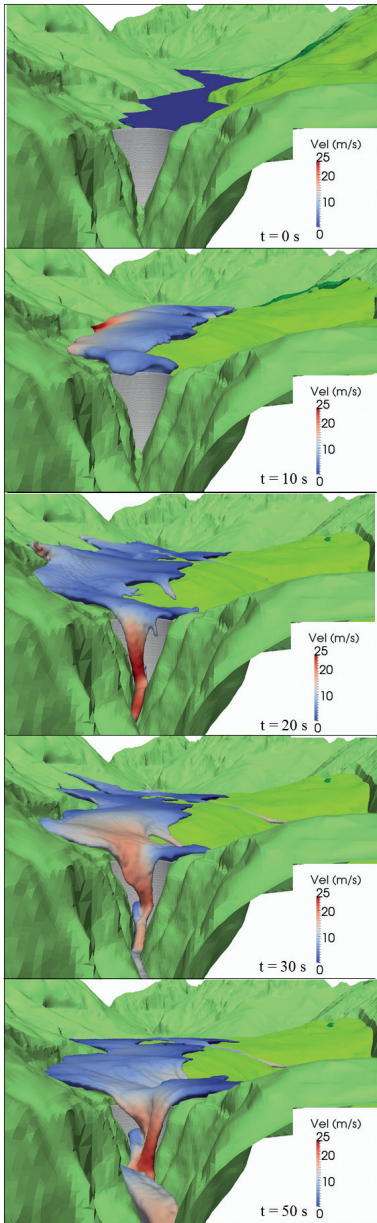


Fig. 8 - Time evolution of the wave and of the velocity module

ble to extend the simulation until the still water condition in the residual lake was reached. The numerical simulation has been interrupted at the physical time equal to 21 minutes (which corresponds to a runtime of 62 hours with an Nvidia GeForce GTX 580 GPU). At this physical time the water stopped flowing from the top of the slide towards east and the volume accumulated in the residual lake was estimated equal to  $78 \cdot 10^6 \text{ m}^3$ . Considering the

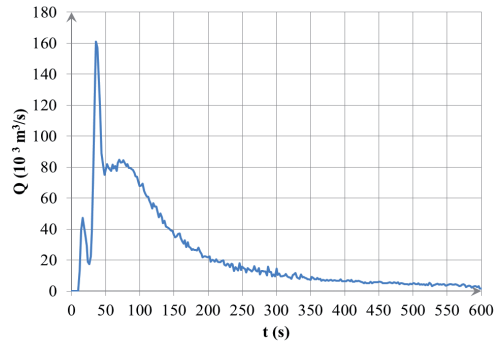


Fig. 9 - Estimated discharge hydrograph overflowing the dam

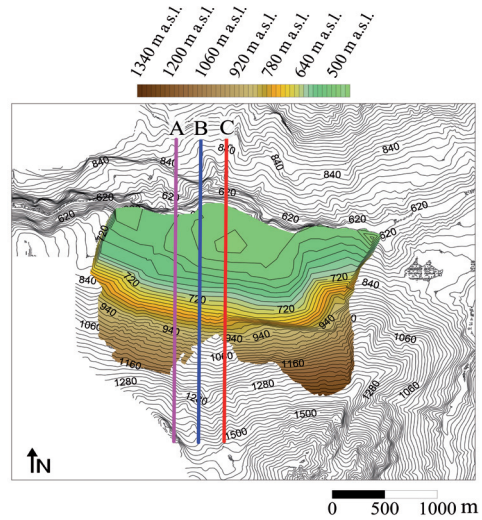


Fig. 10 - Plan traces of the cross-sections A, B, C

stage-volume relationship of the residual lake, the water level corresponding to the total accumulated volume is equal to 710 m a.s.l. This is in good agreement with the data available in literature: SELLI & TREVISAN (1964) and VIPARELLI & MERLA (1968) estimated the level of the residual lake at the end of the events equal to 712 m a.s.l.

The numerical simulations allowed also to reconstruct the discharge hydrograph that overtopped the dam and the neighboring slopes (see Fig. 9). The hydrograph shows two peaks: a small first one at around 15 seconds, with a discharge of about  $50 \cdot 10^3 \text{ m}^3/\text{s}$  and a second one at around 30-40 seconds, with a maximum peak discharge of about  $160 \cdot 10^3 \text{ m}^3/\text{s}$ . The volume of the discharge hydrograph is about  $15 \cdot 10^6 \text{ m}^3$ .

The magnitude and direction of the velocity field in three cross sections (for which the plan traces are reported in Fig. 10) are shown in Fig. 11.

It can be observed that, after 10 seconds, while

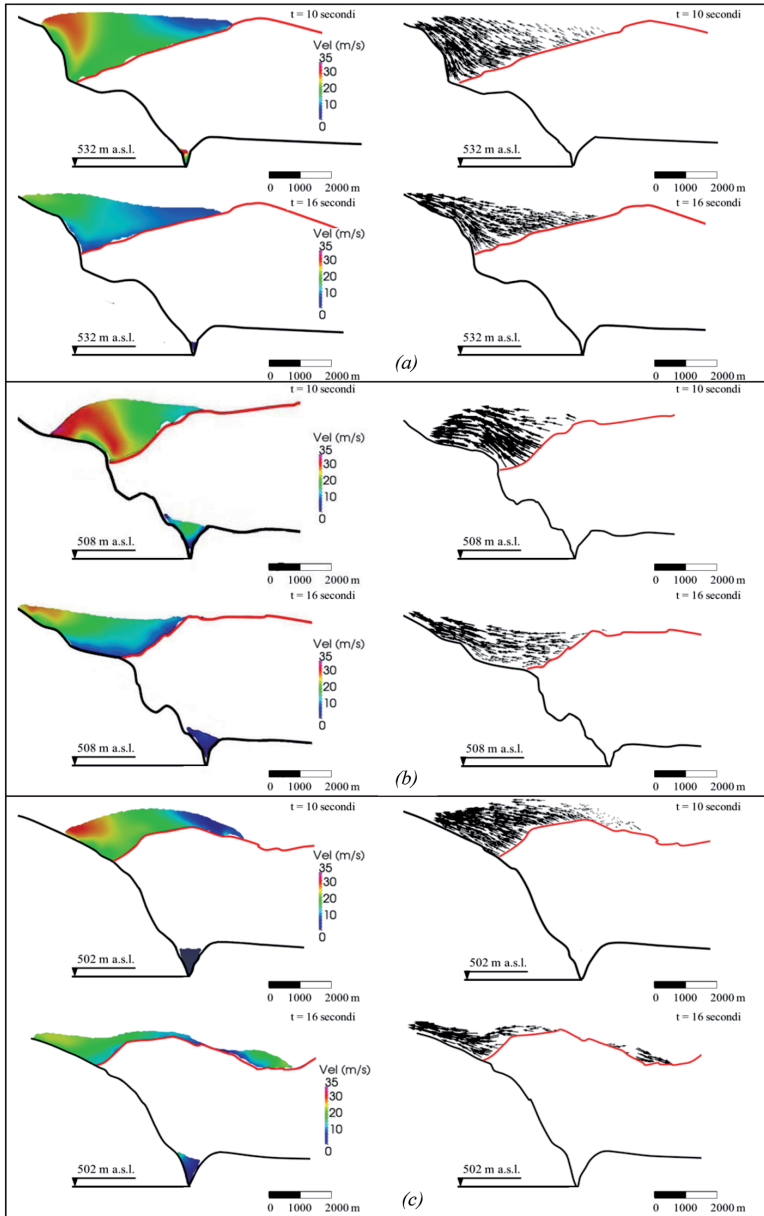


Fig. 11 - Modulus and vectors of the velocity field at the instants 10 and 16 s for cross-section A (a), B (b) and C (c)

the slide is still moving, the water pushed north moves with maximum speeds of 30-35 m/s. After 16 seconds, while the slide is about to stop, the water continues to move toward the north side of the valley.

**CONCLUSION**

In this paper the results of a 3D numerical simulation of the wave generated by the Vajont rockslide

are presented.

To the authors' knowledge this is the first contribution to a complete description of the flow evolution in the artificial lake, including the 3D velocity field and the discharge of the hydrograph which overflowed the dam. The sensitivity analysis of the numerical model has shown that the main parameter which influence the flow dynamics is the total

duration of the fall. In order to correctly reproduce the maximum historical run-up a total duration of the slide movement equal to 17 s is required.

The comparison between the results of the numerical simulation and the data available in literature shows that the numerical scheme is able to reproduce, together with the maximum run-up, also the level in the residual lake after the event.

The numerical results can be adopted in future works as an upstream boundary condition to simu-

late the propagation of the wave in the Vajont gorge, downstream the dam and in the Piave valley.

## ACKNOWLEDGEMENTS

We are grateful to Dr. Alejandro, C. Crespo and Mr. Jose M. Dominguez for the suggestions about the Dualsphysics code. We also want to thank Dr. Laura Superchi for providing the initial data of the slide. The High Performance Computing facilities where provided by the CINECA inter-university consortium.

## REFERENCES

- BACHELOR G.K (1974) - *Introduction to Fluid Dynamics*. Cambridge University Press, UK.
- BOSA S. & PETTI M. (2010) - *Shallow water numerical model of the wave generated by the Vajont landslide*. Environmental Modelling & Software, **26** (4): 406-418.
- CALOI P. (1966) - *L'evento del Vajont nei suoi aspetti geodinamici*. Istituto Nazionale di Geofisica, Roma.
- CIABATTI M. (1964). - *La dinamica della frana del Vajont*. Giornale di Geologia, **32**: 139-160.
- CRESPO A.J.C., GÓMEZ-GESTEIRA M. & DALRYMPLE R.A. (2007) - *Boundary conditions generated by dynamic particles in SPH methods*. Computers, Materials & Continua, **5**: 173-184.
- CRESPO A.J.C., GÓMEZ-GESTEIRA M. & DALRYMPLE R.A. (2008) - *Modeling dam-break behavior over a wet bed by a SPH technique*. Journal of Waterway, Port, Coastal and Ocean Engineering, **134**: 313-320.
- CRESPO A.J.C., DOMINGUEZ J.M., BARREIRO A., GÓMEZ-GESTEIRA M. & ROGERS B.D. (2011) - *GPUs, a New Tool of Acceleration in CFD: Efficiency and Reliability on Smoothed Particle Hydrodynamics Methods*. PLoS ONE, **6**: e20685.
- DALRYMPLE R.A. & ROGERS B.D. (2006) - *Numerical modeling of water waves with the SPH method*. Coastal Engineering, **53**: 141-147.
- DATEI C. (1969) - *Su alcune questioni di carattere dinamico relative ad un eccezionale scoscendimento di un ammasso roccioso*. Memorie della Accademia Patavina, 89-108, Padova.
- DATEI C. (2005) - *Vajont. La storia idraulica*. Cortina, Padova.
- ERISMANN T.H. & ABELE G. (2001) - *Dynamics of rockslides and rockfall*. Springer-Verlag, Berlin-Heidelberg-New York, Berlin.
- GENEVOIS R. & GHIROTTI M. (2005) - *The 1963 Vajont Landslide*. Giornale di Geologia Applicata, **1**: 41-52.
- GINGOLD R.A. & MONAGHAN J.J. (1977) - *Smoothed particle hydrodynamics. Theory and application to non-spherical stars*. Monthly Notices of the Royal Astronomical Society, **181**: 375-389.
- GÓMEZ-GESTEIRA M. & DALRYMPLE R. (2004) - *Using a 3D SPH method for wave impact on a tall structure*. Journal of Waterway, Port, Coastal and Ocean Engineering, **130**: 63-69.
- HENDRON A.J. & PATTON F.D. (1985) - *The Vajont slide, a geotechnical analysis based on new geologic observations of the failure surface*. Engineering Geology, **24**: 479-491.
- LEIMKUHNER B.J., REICH S. & SKEEL R.D. (1996) - *Integration Methods for Molecular dynamic IMA Volume in Mathematics and its application*. Springer.
- MONAGHAN J.J. (1989) - *On the problem of penetration in particle methods*. Journal of Computational Physics, **82**: 1-15.
- MONAGHAN J.J. (1994) - *Simulating free surface flows with SPH*. Journal of Computational Physics, **110**: 399-406.
- MÜLLER L. (1961) - *Talsperre Vajont*. 15° Baugeologischer Bericht: Die Felsgleitung im Bereich Toc. Unpublished technical Report for S.A.D.E, Venezia.
- MÜLLER L. (1987a) - *The Vajont catastrophe - A personal review*. Engineering Geology, **24**: 423-444.
- MÜLLER L. (1987b) - *The Vajont slide*. Engineering Geology, **24**: 513-527.
- SEMENZA E., ROSSI D. & GIUDICI F. (1965) - *Carte geologiche del versante settentrionale del Monte Toc e zone limitrofe, prima e dopo il fenomeno di scivolamento del 9 ottobre 1963*. Scala 1:5000. Istituto di Geologia dell'Università di Padova, Padova.
- SELLI R. & TREVISAN L. (1964) - *Caratteri e interpretazione della Frana del Vajont*. Giornale di Geologia, **32**: 1-154.
- SEMENZA E. (2001) - *La storia del Vajont raccontata dal geologo che ha scoperto la frana*. Tecomproject Ed. Multimediale, Ferrara.

- SEMENZA E. & MELIDORO G. (1992) - *Proceedings of the meeting on the 1963 Vajont landslide*. University of Ferrara, Ferrara.
- SUPERCHI L. (2011) - *The Vajont rockslide: new techniques and traditional method to re-evaluate the catastrophic event*. Ph.D thesis XXIV ciclo, Ph.D School in Earth Sciences, Università di Padova.
- VIPARELLI M. & MERLA G. (1968) - *L'onda di piena seguita alla frana del Vajont*. Atti dell'Accademia Pontaniana, 15.
- WENDLAND H. (1995) - *Piecewise polynomial, positive definite and compactly supported radial functions of minimal degree*. *Advances in Computational Mathematics*, 4: 389-3.